AGU PUBLICATIONS

Geophysical Research Letters

RESEARCH LETTER
10.1002/2014GL060602

Key Points:
- We present a new method for time-lapse seismic monitoring
- We apply the new method to a large industrial data set
- We detect small changes in the subsoil caused by reservoir exploitation

Supporting Information:
- Readme
- Figure S2
- Figure S1

Correspondence to:
N. M. Shapiro,
nshapiro@ipgp.fr

Citation:
Mordret, A., N. M. Shapiro, and S. Singh (2014), Seismic noise-based time-lapse monitoring of the Valhall overburden, *Geophys. Res. Lett.*, *41*, 4945–4952, doi:10.1002/2014GL060602.

Received 20 MAY 2014
Accepted 9 JUL 2014
Accepted article online 12 JUL 2014
Published online 24 JUL 2014

Seismic noise-based time-lapse monitoring of the Valhall overburden

Aurélien Mordret[1], Nikolaï M. Shapiro[1], and Satish Singh[2]

[1]Laboratoire de sismologie, Institut de Physique du Globe de Paris, Sorbonne Paris Cité, Université Paris Diderot, CNRS (UMR 7154), Paris, France [2]Laboratoire de geosciences marines, Institut de Physique du Globe de Paris, Sorbonne Paris Cité, Université Paris Diderot, CNRS (UMR 7154), Paris, France

Abstract We used two "vintages" of ambient seismic noise recorded at the Valhall Life of the Field Seismic network in 2004 and 2005 to perform a passive time-lapse imaging of the subsurface. First, the cross correlations between each pair of stations were computed for both vintages to extract Scholte waves. Second, the relative velocity variations between the 2004 and 2005 cross correlations were measured on the ballistic waves using the Moving-Window Cross-Spectral technique. Finally, the best quality relative velocity variation measurements were regionalized using a modified eikonal tomography technique. The results, albeit noisy because of the short duration of the available records, show a large patch of increased seismic velocity in the southern part of the network and a weaker anomaly in the northern part. The southern increase of velocity can be attributed to the exploitation of the southern flank of the Valhall reservoir with new wells and is in good agreement with a previous time-lapse study using Scholte waves.

1. Introduction

Deterministic signals extracted from cross correlations (CCs) of seismic noise [e.g., *Gouédard et al.*, 2008, and references therein] provide a very attractive alternative to earthquake or active sources. For receivers installed on the Earth's surface, these noise CCs are dominated by fundamental-mode surface waves [e.g., *Shapiro and Campillo*, 2004]. This technique provides two families of applications: the first one is made of noise-based surface wave tomographic methods. It is particularly advantageous within the context of modern seismic arrays where computing the CCs between all pairs of sensors results in very dense and well-distributed path coverage. Noise-based surface wave imaging has been applied at regional and continental scales to infer crustal structures [e.g., *Shapiro et al.*, 2005; *Yao et al.*, 2006; *Yang et al.*, 2008; *Stehly et al.*, 2009; *Lin et al.*, 2009; *Fry et al.*, 2010]. The noise cross-correlation approach has also been applied to continuous records from industrial seismic networks to extract reflection responses [*Draganov et al.*, 2007, 2013] and surface waves [*De Ridder and Biondi*, 2013; *Mordret et al.*, 2013a; *Lin et al.*, 2013].

The second family of applications is based on the permanency and repeatability of the seismic noise and allows the emergence of continuous monitoring methods. Cross correlations of noise can be computed, for example, on a daily basis, and the comparison of the daily waveforms may be used to track the temporal variations of the seismic velocity of the medium between the stations. Noise-based monitoring methods generally have a better temporal resolution and repeatability compared to methods based on earthquake doublets. These monitoring methods have been successfully applied on volcanoes [*Sens-Schönfelder and Wegler*, 2006; *Brenguier et al.*, 2008a; *Duputel et al.*, 2009; *Mordret et al.*, 2010], active faults [e.g., *Wegler and Sens-Schonfelder*, 2007; *Brenguier et al.*, 2008b; *Chen et al.*, 2010; *Zaccarelli et al.*, 2011] and landslides [*Mainsant et al.*, 2012].

Noise-based monitoring may be of major interest for industrial applications. However, a very few studies have been undertaken in this context so far [e.g., *Corciulo et al.*, 2012; *Delatre and Manceau*, 2013; *De Ridder and Biondi*, 2013]. In the present paper, data of the Valhall Life of Fields Seismic network (LoFS, Figure 1a) have been used to extract Scholte waves (i.e., waves traveling along the interface of a water layer and the subbottom sediments) from cross correlation of ambient seismic noise. The Valhall LoFS permanent network operated by BP Norge A/S was installed on the North Sea seafloor in 2003 over the Valhall oil field. The network covers 70% of the field area and is made of 120 km of ocean bottom cables buried at 1 m depth in the soil where data are continuously recorded by 2320 four-component seismic sensors (4C: Up, North, East, and Hydrophone) [e.g., *VanGestel et al.*, 2008; *De Ridder and Dellinger*, 2011; *Mordret et al.*, 2013a].

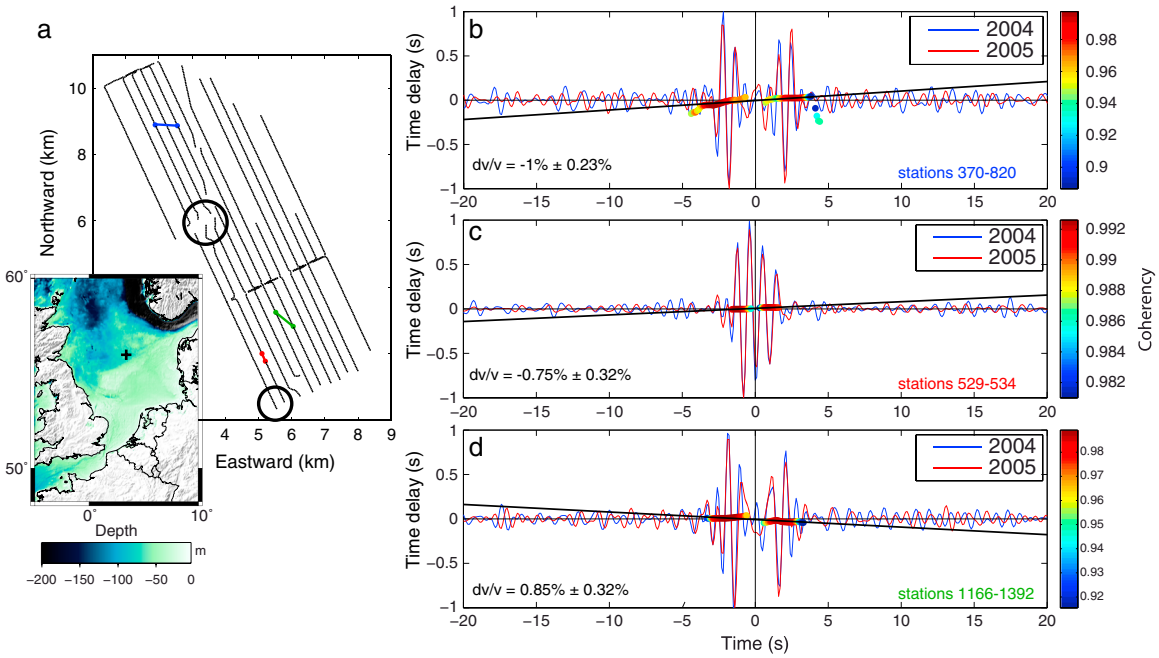

Figure 1. Example of relative velocity variation measurements. (a) Map and location of the Valhall seismic network. Each black point represents a 4C sensor. The black circles show the approximate positions of the exploitation platforms. The red points are stations 529 and 534, the blue points are stations 370 and 820, and the green points are stations 1166 and 1392. The insets show the geographical location of the Valhall field with the black cross showing the location of the Valhall LoFS array. The bathymetry is shown as the background of the right inset. (b–d) Three examples of relative velocity variation measurements. The colored circles show the time delays measured with the Moving-Window Cross-Spectral technique, the color representing the coherency of the two waveforms in each moving window. The black line shows the weighted linear fit to the time delays. The relative velocity variation and its uncertainty are shown in each panel.

We used two data sets, the first one was recorded in 2004 during 29 h and the second one was recorded in 2005 during 6.5 h, to compute a time-lapse image of the velocity changes during the year between these measurements.

2. Data and Noise Cross Correlations

We analyzed the continuous signals recorded at 250 Hz from 2320 sensors of the LoFS network. The CCs computation is described in detail by *Mordret et al.* [2013a] for the 2005 data set and partly follows the workflow of *Bensen et al.* [2007], involving downsampling to 10 Hz, spectral whitening between 0.62 and 2.5 s before computing the CCs. The same processing has been applied to the 2004 data set. Because the data did not present strong amplitude variations, we did not use temporal normalization. In this study, we focused on Scholte waves and used the ZZ cross correlations from all station pairs, that is, 2690040 CCs.

Mordret et al. [2013a] showed that the ambient noise recorded during the considered 6 h in 2005 is strongly affected by two operating platforms: one in the center of the network and another one at the south (Figure 1). The noise source distribution was found homogeneous only for the 0.62 s–2.5 s period band, where the CCs were symmetric. At shorter periods, the exploitation platforms act as a strongly dominant localized noise point source preventing the convergence of the CCs toward Green's functions for most of the station pairs. Therefore, we only analyze here the CCs above 0.62 s that contain reconstructed Scholte waves from natural well-distributed noise.

As shown in the three examples of Figures 1b–1d, the waveform similarity between the 2004 and 2005 data set is relatively low, the coda parts of the CCs being strongly decorrelated whereas the direct arrivals being more similar. Two causes can produce such differences. First, if the medium beneath the sensors has drastically changed between the two data acquisitions, the waveforms can be distorted. The coda parts of the cross correlations being more sensitive to changes than the direct arrivals [*Snieder et al.*, 2002; *Brenguier et al.*, 2011], it would be normal to observe that they are more decorrelated than the direct waves. The second and more likely cause could be the too short recording duration of the data sets. It is possible that 29 h

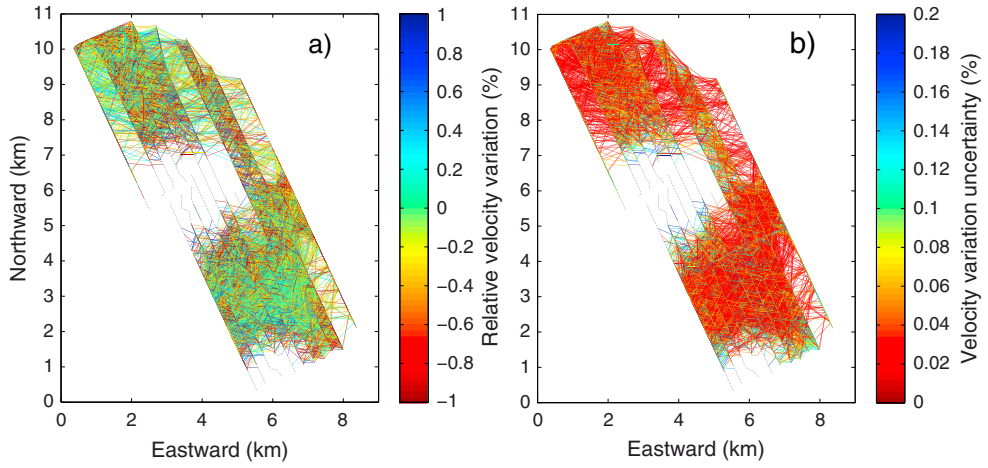

Figure 2. Results of relative velocity variation measurements for all cross correlations used in this study. (a) Relative velocity variations $\delta v/v$. (b) Error of the relative velocity variations σ_{slope} [*Clarke et al.*, 2011].

of noise for the 2004 data set and in a larger extent 6.5 h of noise for the 2005 data set are not enough to reconstruct full Green's functions and that only their direct arrivals are properly recovered.

3. Relative Velocity Variation Measurements and Eikonal Time-Lapse Imaging

The Moving-Window Cross-Spectral (MWCS) technique [*Poupinet et al.*, 1984; *Brenguier et al.*, 2008a; *Clarke et al.*, 2011] is used to infer the velocity changes between 2004 and 2005. We follow the procedure developed by *Clarke et al.* [2011]. Unlike most studies using noise cross correlation for monitoring velocity changes, the time delays are computed only within the direct arrival windows defined by velocities between 200 m/s and 1000 m/s. The moving window used for the measurements is 4 s wide and moves with 0.05 s steps. The measurements are done in the 0.62 to 1.25 s period band where the signal-to-noise ratio is the highest. For every window, the measured time delay δt is associated to a standard error $\sigma_{\delta t}$. To infer the relative time shift $\delta t/t$, a linear regression is fitted to the time delay measurements from windows exhibiting a coherency higher than 0.875. The error on the slope, σ_{slope}, of the linear regression is also evaluated [*Clarke et al.*, 2011]. The relative velocity variation is then the opposite of the relative time shift

$$\frac{\delta v}{v} = -\frac{\delta t}{t}. \tag{1}$$

The absolute time delay $\delta t_{0.8s}$ between the direct Scholte waves is computed as

$$\delta t_{0.8s} = \left(\frac{\delta t}{t}\right) t_{0.8s}, \tag{2}$$

where $t_{0.8s}$ is the travel time of the direct Scholte wave at 0.8 s, center of the studied period band. This travel time is measured from the Scholte wave velocity map at 0.8 s from *Mordret et al.* [2013b]. Figures 1b–1d show three examples of relative velocity variation measurement and their errors. Our analysis shows that it is possible to measure relative velocity variations with small uncertainties.

Figure 2a shows the relative velocity variation measurements for the CCs used in this study, that is, the station pairs from which the interstation distance is longer than 0.33 km (about one wavelength) and the correlation coefficient of the direct arrival window between the pair of waveform is higher than 0.9. Figure 2b shows the errors σ_{slope} associated with these measurements. The areas around the platforms have no data. Far from the platforms, the average relative velocity variation is close to $\pm$0.3% with errors on the order of 0.03%.

To have a better estimate of the spatial distribution of the velocity changes, a tomographic technique is used to regionalize these values. To proceed, we modified the eikonal tomography technique [*Lin et al.*, 2009] to adapt it to time delay measurements. We started from a 2-D eikonal equation

$$\vec{\nabla} t = s\mathbf{k}, \tag{3}$$

where $\vec{\nabla}$ is the gradient, t is the travel time, s is the slowness of Scholte waves, and $\mathbf{k}$ is the unit wave number vector. This equation can be adapted to time delays, assuming the angle between $\vec{\nabla} t_{2004}$ and $\vec{\nabla} t_{2005}$ is small

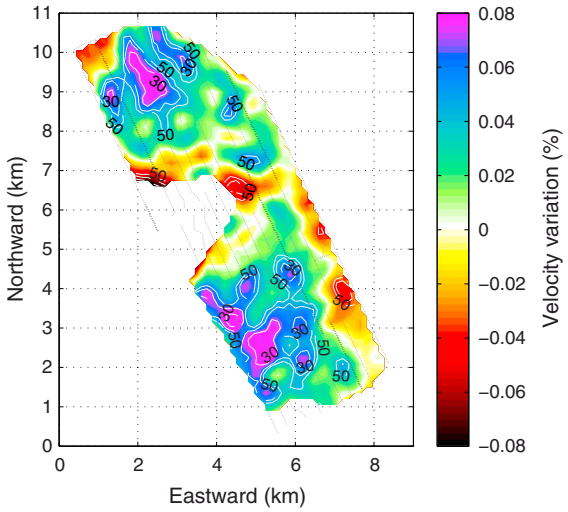

Figure 3. Relative velocity variations regionalized with the eikonal time-lapse method. Only the $\delta v/v$ measurements with interstation distances longer than 0.33 km and pairs of 2004–2005 CCs with correlation coefficients of the direct arrival window higher than 0.9 are used. The contours show the relative errors from 30% to 50% with 10% steps. Areas with errors less than 50% are considered reliable.

enough, i.e., the velocity variations are homogeneous in space (see Figure S1 in the supporting information for a graphical demonstration):

$$\delta s = |\vec{\nabla} t_{2005}| - |\vec{\nabla} t_{2004}| \simeq \frac{\vec{\nabla}\delta t \cdot \vec{\nabla} t_{2004}}{|\vec{\nabla} t_{2004}|} \quad (4)$$

with $\delta t = t_{2005} - t_{2004}$ and $\delta s = s_{2005} - s_{2004}$, the travel time and slowness differences between 2005 and 2004, respectively, and the dot in the numerator of the right-hand side denoting the dot product between two vectors.

If we assume a smooth distribution of seismic velocities, we can assume that the trajectory of the direct waves follows a straight ray. Therefore, the directions of propagation from the virtual source to each point of the medium can be approximated by the distance vector $\vec{\mathbf{D}}$ between the source and each point of the medium (this approximation can be avoided if $\vec{\nabla} t_{2004}$ is explicitly computed). The slowness variation δs is then

$$\delta s \simeq \frac{\vec{\nabla}\delta t \cdot \vec{\mathbf{D}}}{|\vec{\mathbf{D}}|}. \quad (5)$$

To compute the spatial gradient in equation (5), δt must be interpolated between the measurement points in order to obtain a time delay estimation for each point of the medium. Following *Lin et al.* [2009] and *Mordret et al.* [2013b], the time delay measurements from each virtual source are interpolated on a grid composed of 77×60 square cells with a grid size of 150 m. The interpolation is performed with a cubic spline interpolator with a regularization term based on the curvature of the interpolated surface called tension. A large tension of 0.9999 is used in order to strongly smooth the interpolated surface. We chose a large tension because the discrete time delay measurements present relatively scattered values. By smoothing the interpolated time delay surface, we prevent the spatial gradient having spurious oscillations which would hide the time-lapse signal. The slowness variation surfaces (i.e., the spatial gradient of the time delay surfaces) from each virtual source provide a set of slowness measurements for each point of the medium. These slowness variation distributions are converted into relative velocity variation distributions using a phase velocity map at 0.8 s, $v_{i,0.8s}$, from *Mordret et al.* [2013b] following this relationship

$$\left(\frac{\delta v}{v}\right)_{ir} = -v_{i,0.8s}\,\delta s_i\,. \quad (6)$$

where the subscript i indicates the model grid cell index and r indicates the regionalized value to be distinguished from the relative velocity variation measurements used in equations (1) and (2). We chose a phase velocity map at 0.8 s because it is the central period of the time delay measurements. The final velocity variation map is obtained as the mean of the velocity variation distribution at each point of the grid, and its uncertainty is related to the relative standard error of the mean.

Figure 3 shows the map of $(\delta v/v)_r$. The main features observed are the patch of strong increased velocity in the southern part of the field and a weaker one in the northern part. A weak line of velocity decrease is observed on the eastern side of the network. The white contours show the relative standard errors. We interpret as reliable the areas of the map where the errors are less than 50%.

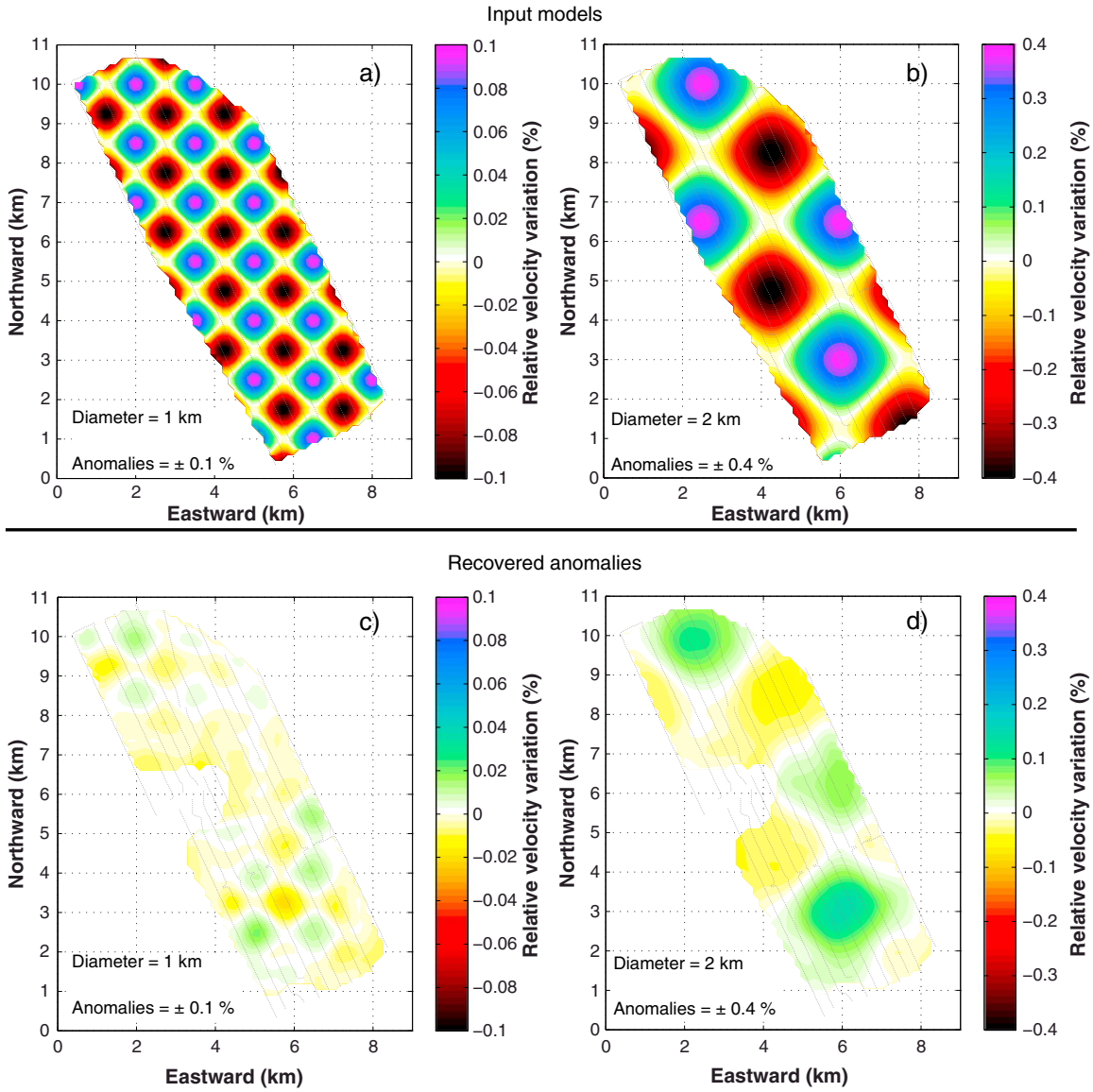

Figure 4. Eikonal time-lapse resolution tests. The input patterns and the results. (a) Input model with 1 km radius relative velocity variation anomalies and 0.1% velocity variation, (b) with 2 km radius anomalies and 0.4% velocity variation. Results of the tests for (c) the 1 km anomalies and (d) the 2 km anomalies. Note how the anomalies are disturbed or attenuated close to the platforms and on the eastern edge of the network.

4. Discussion and Conclusion

We performed resolution tests to assess the reliability of the method. The phase velocity map at 0.8 s from *Mordret et al.* [2013b] has been used to compute the reference travel time between each source and every point of the medium using a fast marching method [*Sethian*, 1996] taking into account bent rays. Then, this velocity map has been perturbed by different velocity variations with a sinusoidal pattern (diameters of 1 km with perturbations of ± 0.1% and diameters of 2 km with perturbations of ± 0.4%) where new travel times have been computed. The difference between the perturbed and unperturbed travel time gave the synthetic time delays used in the inversion procedure. Each synthetic time delay measurement is contaminated with a Gaussian noise with standard deviation equal to the real relative velocity variation uncertainty σ_{slope} shown in Figure 2b of the corresponding time delay measurement.

Figure 4 shows two of these synthetic tests with a different size of relative velocity variation patches. The results of the synthetic tests show that the eikonal time-lapse method with selected interpolation parameters underestimates the actual $\delta v/v$ by a factor ~5 for large-scale perturbations and by a factor ~10 for

small-scale perturbations because of a strong smoothing. The real velocity variation values should therefore be around ± 0.3–0.7%, in good agreement with the individual measurements shown in Figure 2a. The synthetic results also confirm that the areas around the platforms are not resolved and that the values obtained there should not be interpreted. The synthetic tests demonstrate that the large patch of increased velocity at the south of the network is the most robust feature resolved by passive time-lapse imaging, as shown in Figure 4d.

Waveform analysis methods such as the MWCS technique mostly rely on far-field approximations. In this study, the relative velocity variation measurements are performed at distances larger than one wavelength (≈0.33 km), but most of them remain below three wavelengths (see Figure S2 in the supporting information for the distance distribution of the data with respect to the correlation coefficient). We conducted some tests to systematically assess the influence of our data selection criteria, that is, the minimum distance kept for the inversion as well as the influence of the minimum correlation coefficient. It appears that the southern patch of velocity increase is particularly robust with respect to the offset and the correlation coefficient. However, the northern velocity increase can be only retrieved with using measurements from closely located station pairs (see Figure S3 in the supporting information for the results of the different tests).

Our results can be compared with the study by *De Ridder* [2014] who computed time lapse in the model domain between data acquired 7 years apart and with *Wills et al.* [2008] and *Hatchell et al.* [2009] who measured by cross correlation the time shift between Scholte waves acquired during active surveys in November 2003 and November 2005. Even if the methods, the delays between the surveys, and the frequency of the studied waves are different, relative velocity variation retrieved in our study are in good agreement with results from other active surveys and noise-based differential tomography results.

Of particular interest is the area of increased velocity at the south of the field. It is related to the drilling of new wells in 2003 to exploit the southern flank of the reservoir. The previous 20 years of exploitation of the reservoir in the central area has produced a strong subsidence of the seafloor due to the compaction of the rocks in the reservoir [*Hatchell et al.*, 2009]. This subsidence (∼20 cm/yr) is not uniform and creates a bowl with compaction at the center and strong extension on the edges. This extension opens concentric cracks that produce noticeable azimuthal anisotropy [*Barkved and Kristiansen*, 2005; *Mordret et al.*, 2013c]. When the exploitation started on the southern flank, a new small subsidence bowl started to form on the edge of the older one which closed the former cracks and tend to increase the seismic velocity. The same time-lapse pattern is found in P-to-S converted waves time shift and shear wave splitting delay measurements [*Zwartjes et al.*, 2008]. Most likely, the northern patch of increased velocity is also related to the subsidence.

We show in this study that the ambient noise cross-correlation method could be used in a marine and industrial environment to produce time-lapse maps of the Scholte waves relative velocity variations from data sets recorded 1 year apart. At Valhall, 6.5 h of continuous noise are sufficient to accurately reconstruct the direct arrivals of Scholte waves, but the robustness of the results would greatly benefit from having longer noise records. At periods around 1 s, the Scholte waves in the cross correlations have a sensitivity down to few hundreds of meters. Provided a dense seismic network like Valhall LoFS, this passive technique could then be used to monitor and locate the changes in the shallow subsurface in quasi real time.

This passive eikonal time-lapse technique could also be complementary to interferometric synthetic aperture radar (InSAR) measurements to monitor and locate small-scale deformations. We believe that this technique could have important applications in monitoring of hydrocarbon reservoirs [e.g., *Xu et al.*, 2001], CO_2 sequestration reservoirs [e.g., *Vasco et al.*, 2008], mining environments [e.g., *Carnec and Delacourt*, 2000], or sinkholes [e.g., *Closson et al.*, 2005]. It could also be applied at locations where InSAR cannot be implemented like marine or vegetation-covered areas.

Acknowledgments
We thank BP Norge AS and the Valhall partner, Hess Norge AS, for granting access to the seismic data. The authors also acknowledge Joe Dellinger who prepared the data as well as the use of resources provided by the European Grid Infrastructure. For more information, please consult the EGI-InSPIRE paper (http://go.egi.eu/pdnon). The contribution of A.M. and N.S. was supported by a FP7 ERC Advanced grant 227507 (WHISPER); A.M. and N.S. also acknowledge the support from the DataScale project. The authors thank two reviewers Sjoerd de Ridder and Kees Wapenaar as well as the Associate Editor for their comments and suggestions which helped to drastically improve the quality of this paper. This is IPGP contribution 3546.

The Editor thanks Sjoerd de Ridder and Kees Wapenaar for their assistance in evaluating this paper.

References

Barkved, O., and T. Kristiansen (2005), Seismic time-lapse effects and stress changes: Examples from a compacting reservoir, *Leading Edge*, *24*, 1244–1248.

Bensen, G., M. Ritzwoller, M. Barmin, A. Levshin, F. Lin, M. Moschetti, N. M. Shapiro, and Y. Yang (2007), Processing seismic ambient noise data to obtain reliable broad-band surface wave dispersion measurements, *Geophys. J. Int.*, *169*(3), 1239–1260.

Brenguier, F., N. M. Shapiro, M. Campillo, V. Ferrazzini, Z. Duputel, O. Coutant, and A. Nercessian (2008a), Towards forecasting volcanic eruptions using seismic noise, *Nat. Geosci.*, *1*, 126–130, doi:10.1038/ngeo104.

Brenguier, F., M. Campillo, C. Hadziioannou, N. M. Shapiro, R. Nadeau, and E. Larose (2008b), Postseismic relaxation along the San Andreas Fault at Parkfield from continuous seismological observations, *Science*, *321*(5895), 1478–1481, doi:10.1126/science.1160943.

Brenguier, F., D. Clarke, Y. Aoki, N. M. Shapiro, M. Campillo, and V. Ferrazzini (2011), Monitoring volcanoes using seismic noise correlations, *C. R. Geosci.*, *343*(8), 633–638.
Carnec, C., and C. Delacourt (2000), Three years of mining subsidence monitored by SAR interferometry, near Gardanne, France, *J. Appl. Geophys.*, *43*(1), 43–54.
Chen, J. H., B. Froment, Q. Y. Liu, and M. Campillo (2010), Distribution of seismic wave speed changes associated with the 12 May 2008 Mw 7.9 Wenchuan earthquake, *Geophys. Res. Lett.*, *37*, L18302, doi:10.1029/2010GL044582.
Clarke, D., L. Zaccarelli, N. M. Shapiro, and F. Brenguier (2011), Assessment of resolution and accuracy of the Moving Window Cross Spectral technique for monitoring crustal temporal variations using ambient seismic noise, *Geophys. J. Int.*, *186*, 867–882.
Closson, D., N. A. Karaki, Y. Klinger, and M. J. Hussein (2005), Subsidence and sinkhole hazard assessment in the southern Dead Sea area, Jordan, *Pure Appl. Geophys.*, *162*(2), 221–248.
Corciulo, M., P. Roux, M. Campillo, and D. Dubucq (2012), Instantaneous phase variation for seismic velocity monitoring from ambient noise at the exploration scale, *Geophysics*, *77*(4), Q37–Q44.
Delatre, M., and J.-C. Manceau (2013), Applicability of long-range seismic noise correlation for CO_2 geological storage monitoring, *Energy Procedia*, *37*, 4049–4056.
De Ridder, S., and B. Biondi (2013), Daily reservoir-scale subsurface monitoring using ambient seismic noise, *Geophys. Res. Lett.*, *40*, 2969–2974, doi:10.1002/grl.50594.
De Ridder, S., and J. Dellinger (2011), Ambient seismic noise eikonal tomography for near-surface imaging at Valhall, *Leading Edge*, *30*(5), 506–512.
De Ridder, S. A. L. (2014), Passive seismic surface-wave interferometry for reservoir-scale imaging, PhD thesis, Stanford Univ., Stanford, Calif.
Draganov, D., K. Wapenaar, W. Mulder, J. Singer, and A. Verdel (2007), Retrieval of reflections from seismic background-noise measurements, *Geophys. Res. Lett.*, *34*, L04305, doi:10.1029/2006GL028735.
Draganov, D., X. Campman, J. Thorbecke, A. Verdel, and K. Wapenaar (2013), Seismic exploration-scale velocities and structure from ambient seismic noise (> 1 hz), *J. Geophys. Res. Solid Earth*, *118*, 4345–4360, doi:10.1002/jgrb.50339.
Duputel, Z., V. Ferrazzini, F. Brenguier, N. M. Shapiro, M. Campillo, and A. Nercessian (2009), Real time monitoring of relative velocity changes using ambient seismic noise at the Piton de la Fournaise volcano (La Réunion) from January 2006 to June 2007, *J. Volcanol. Geotherm. Res.*, *184*(1–2), 164–173.
Fry, B., F. Deschamps, E. Kissling, L. Stehly, and D. Giardini (2010), Layered azimuthal anisotropy of Rayleigh wave phase velocities in the European Alpine lithosphere inferred from ambient noise, *Earth Planet. Sci. Lett.*, *297*(1), 95–102.
Gouédard, P., et al. (2008), Cross-correlation of random fields: Mathematical approach and applications, *Geophys. Prospect.*, *56*(3), 375–393.
Hatchell, P., P. Wills, and C. Didraga (2009), Production induced effects on near-surface wave velocities at Valhall, in *71st EAGE Conference and Exhibition,* EAGE, Extended Abstracts, p. T016.
Lin, F., M. Ritzwoller, and R. Snieder (2009), Eikonal tomography: Surface wave tomography by phase front tracking across a regional broad-band seismic array, *Geophys. J. Int.*, *177*(3), 1091–1110.
Lin, F.-C., D. Li, R. W. Clayton, and D. Hollis (2013), High-resolution 3D shallow crustal structure in Long Beach, California: Application of ambient noise tomography on a dense seismic array, *Geophysics*, *78*(4), Q45–Q56.
Mainsant, G., E. Larose, C. Brönnimann, D. Jongmans, C. Michoud, and M. Jaboyedoff (2012), Ambient seismic noise monitoring of a clay landslide: Toward failure prediction, *J. Geophys. Res.*, *117*, F01030, doi:10.1029/2011JF002159.
Mordret, A., A. Jolly, Z. Duputel, and N. Fournier (2010), Monitoring of phreatic eruptions using interferometry on retrieved cross-correlation function from ambient seismic noise: Results from Mt. Ruapehu, New Zealand, *J. Volcanol. Geotherm. Res.*, *191*(1–2), 46–59.
Mordret, A., M. Landès, N. Shapiro, S. Singh, P. Roux, and O. Barkved (2013a), Near-surface study at the Valhall oil field from ambient noise surface wave tomography, *Geophys. J. Int.*, *193*(3), 1627–1643.
Mordret, A., N. M. Shapiro, S. C. Singh, P. Roux, and O. I. Barkved (2013b), Helmholtz tomography of ambient noise surface wave data to estimate Scholte wave phase velocity at Valhall Life of the Field, *Geophysics*, *78*(2), WA99–WA109.
Mordret, A., N. M. Shapiro, S. Singh, P. Roux, J.-P. Montagner, and O. Barkved (2013c), Azimuthal anisotropy at Valhall: The Helmholtz equation approach, *Geophys. Res. Lett.*, *40*, 2636–2641, doi:10.1002/grl.50447.
Poupinet, G., W. Ellsworth, and J. Frechet (1984), Monitoring velocity variations in the crust using earthquake doublets: An application to the Calaveras Fault, California, *J. Geophys. Res.*, *89*(B7), 5719–5731.
Sens-Schönfelder, C., and U. Wegler (2006), Passive image interferometry and seasonal variations of seismic velocities at Merapi Volcano, Indonesia, *Geophys. Res. Lett.*, *33*, L21302, doi:10.1029/2006GL027797.
Sethian, J. A. (1996), A fast marching level set method for monotonically advancing fronts, *Proc. Natl. Acad. Sci.*, *93*(4), 1591–1595.
Shapiro, N. M., and M. Campillo (2004), Emergence of broadband Rayleigh waves from correlations of the ambient seismic noise, *Geophys. Res. Lett.*, *31*, 1615–1619, doi:10.1029/2004GL019491.
Shapiro, N. M., M. Campillo, L. Stehly, and M. Ritzwoller (2005), High-resolution surface-wave tomography from ambient seismic noise, *Science*, *307*(5715), 1615–1618.
Snieder, R., A. Grêt, H. Douma, and J. Scales (2002), Coda wave interferometry for estimating nonlinear behavior in seismic velocity, *Science*, *295*(5563), 2253–2255.
Stehly, L., B. Fry, M. Campillo, N. M. Shapiro, J. Guilbert, L. Boschi, and D. Giardini (2009), Tomography of the Alpine region from observations of seismic ambient noise, *Geophys. J. Int.*, *178*(1), 338–350.
VanGestel, J.-P., J. H. Kommedal, O. I. Barkved, I. Mundal, R. Bakke, and K. D. Best (2008), Continuous seismic surveillance of Valhall Field, *Leading Edge*, *27*(12), 1616–1621, doi:10.1190/1.3036964.
Vasco, D., A. Ferretti, and F. Novali (2008), Reservoir monitoring and characterization using satellite geodetic data: Interferometric synthetic aperture radar observations from the Krechba field, Algeria, *Geophysics*, *73*(6), WA113–WA122.
Wegler, U., and C. Sens-Schonfelder (2007), Fault zone monitoring with passive image interferometry, *Geophys. J. Int.*, *168*(3), 1029–1033.
Wills, P., P. Hatchell, and S. Bourne (2008), Time-lapse measurements of shallow horizontal wave velocity over a compacting field, in *70th EAGE Conference and Exhibition,* EAGE, Extended Abstracts, p. G039.
Xu, H., J. Dvorkin, and A. Nur (2001), Linking oil production to surface subsidence from satellite radar interferometry, *Geophys. Res. Lett.*, *28*(7), 1307–1310.
Yang, Y., M. H. Ritzwoller, F.-C. Lin, M. Moschetti, and N. M. Shapiro (2008), Structure of the crust and uppermost mantle beneath the western United States revealed by ambient noise and earthquake tomography, *J. Geophys. Res.*, *113*, B12310, doi:10.1029/2008JB005833.

Yao, H., R. Van Der Hilst, and M. De Hoop (2006), Surface-wave array tomography in SE Tibet from ambient seismic noise and two-station analysis–I. Phase velocity maps, *Geophys. J. Int.*, *166*(2), 732–744.

Zaccarelli, L., N. Shapiro, L. Faenza, G. Soldati, and A. Michelini (2011), Variations of crustal elastic properties during the 2009 l'aquila earthquake inferred from cross-correlations of ambient seismic noise, *Geophys. Res. Lett.*, *38*, L24304, doi:10.1029/2011GL049750.

Zwartjes, P., P. Wills, J. De Maag, and P. Hatchell (2008), Shallow and deep time-lapse effects on Valhall LoFS converted wave data, in *70th EAGE Conference and Exhibition,* EAGE, Extended Abstracts, p. G040.